Large spontaneous magnetostriction in $FeTiO_3$ and adjustable magnetic configuration in Fe(III)-doped $FeTiO_3$

M. Charilaou,[1,2,*] D. Sheptyakov,[3] J. F. Löffler,[2] and A. U. Gehring[1]

[1]*Earth and Planetary Magnetism, Department of Earth Sciences, ETH Zurich, 8092 Zurich, Switzerland*

[2]*Laboratory of Metal Physics and Technology, Department of Materials, ETH Zurich, 8093 Zurich, Switzerland*

[3]*Laboratory for Neutron Scattering, Paul Scherrer Institute, 5232 Villigen, Switzerland*

(Received 1 December 2011; published 30 July 2012)

We present neutron diffraction data and magnetic susceptibility measurements of $FeTiO_3$ ilmenite and Fe(III)-doped ilmenites (with 10 and 20 mol. % Fe_2O_3) at temperatures of 1.9 K $< T <$ 300 K. The magnetic moments of the Fe cations in $FeTiO_3$ lie predominantly along the c axis, with a weak component in the lateral layers. With increasing Fe(III) doping the component in the lateral layers grows and the magnetic moments are tilted inside the layers. The lattice dimensions decrease with decreasing temperature, but upon the onset of magnetic long-range order they grow strongly and $FeTiO_3$ exhibits large spontaneous magnetostriction in the per-mille range along the c axis at $T = 1.9$ K. In the Fe(III)-doped ilmenites the spontaneous magnetostriction is negligible, but application of an external field at low temperature causes a strong reduction in the unit cell dimensions as the magnetic layer configuration is changed. This is also seen in the macroscopic magnetic moment, which increases by two orders of magnitude if cooled with a magnetic field, whereas the field-cooled state exhibits a self-reversal upon heating.

DOI: 10.1103/PhysRevB.86.024439 PACS number(s): 75.47.Lx, 75.25.−j, 75.80.+q

I. INTRODUCTION

The effect of magnetostriction, i.e., the change of dimensions with applied magnetic field or upon magnetic ordering, has been studied extensively over the past 100 years.[1,2] Macroscopic magnetostriction due to an applied field has found widespread application in actuators and sensors. The macroscopic effects are usually interpreted in terms of micromagnetic effects, i.e., domain-wall movements. In contrast, the intrinsic spontaneous magnetostriction, where the internal crystal structure changes with temperature in the absence of an external field, is still not well understood, partially because it is material specific. Such intrinsic phenomena, often described as Invar anomalies,[3] have been observed in various intermetallic compounds,[4–9] rare-earth metals,[1,10,11] and rare-earth compounds.[12,13] Over the years major theoretical efforts have been undertaken towards explaining the underlying mechanisms of these phenomena.[14–21] In this study, we present neutron diffraction data for the antiferromagnet $FeTiO_3$ and the ferrimagnetic $(x)FeTiO_3$-$(1-x)Fe_2O_3$ solid solutions with $x = 0.9$ and 0.8, which reveal large spontaneous magnetostriction below their ordering temperature.

The crystal and magnetic structure of $FeTiO_3$ ilmenite and its solid solutions with Fe_2O_3 hematite have attracted considerable interest in physics,[22–26] the Earth sciences,[27–29] and materials science.[30,31] The compound $FeTiO_3$ is an antiferromagnet with a Néel temperature of $T_N = 58(1)$ K[23] and a semiconductor with a measured band gap of $E_g = 2.5$ eV.[32,33] It crystallizes in the $R\bar{3}$ structure (see Fig. 1), where Fe(II) and Ti(IV) are octahedrally coordinated by oxygen and are partitioned into layers.[22,27] The coordination octahedra around Fe(II) and Ti(IV) in neighboring layers are sharing either faces or corners, while within layers the octahedra are sharing edges. The solid solutions with hematite also order in the $R\bar{3}$ symmetry, depending on the quenching temperature.[34,35] The Ti-rich solid solutions ($x \geqslant 0.8$) exhibit ferrimagnetic behavior with a Curie temperature which is nearly linear to the composition x[36,37] and at low temperature ($T < 50$ K) have a freezing transition during which the spin configuration changes in a spin-glass-like fashion due to the frustration in the system.[38–42]

Frustration, a state resulting from unfulfilled demands, occurs in diverse systems where competing interests of interacting parties cannot be simultaneously satisfied. The large number of conflicting interactions hinders the predictability and control of the overall macroscopic properties. Well-known examples of frustrated systems are magnets where spins cannot align in long-range order,[43–47] glasses where atoms of different species fail to form crystals,[48–50] and ferroelectric materials where competing degrees of polarization form glassy states.[51–53] In magnetic systems, frustration arises from competing exchange interactions between single spins generating complex energy landscapes,[54–61] which generally prevent long-range ordering and may lead to exotic states, such as spin glasses and spin liquids. In contrast to spin glasses and spin liquids, which have, in principle, only short-range order, certain materials reveal long-range magnetic order despite frustration. This is possible if the frustration is organized, i.e., the competition is between collective spin partitions and is located in specific symmetries in the system. Such systems with frustrated long-range order are an excellent test bed for deeper investigations of fundamental aspects of frustration, i.e., energy-balance competition.

Members of the hemo-ilmenite solid solution series with $x \geqslant 0.8$ are an excellent example of this class of materials.[28,39,42] The cationic setup in the system generates Fe-rich (A) and Fe-deficient (B) alternating layers. Inside each layer, the spins of the Fe ions prefer parallel alignment due to direct exchange interactions,[62] but spins from neighboring layers show different behavior. Fe(II) spins in subsequent A layers in ilmenite order antiparallel to each other due to the oxygen-induced superexchange, and thus have a modulation of 4 crystalline layers;[23,63] Fe(III) spins, however, exhibit a modulation of 2 crystalline layers as in the end-member hematite.[64] Hence the system demonstrates layer-wise

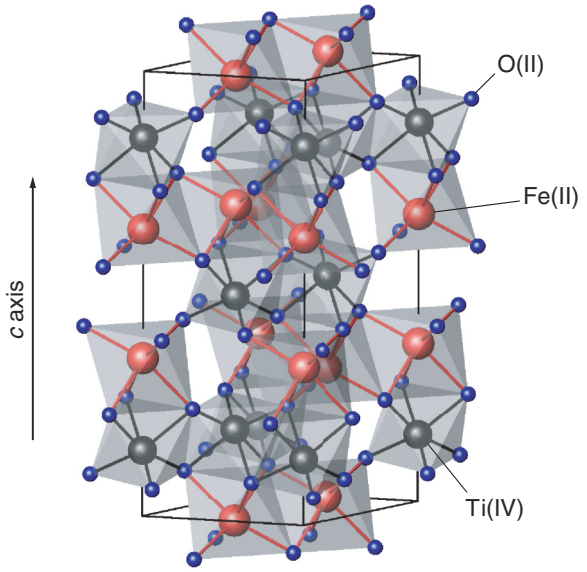

FIG. 1. (Color online) $R\bar{3}$ structure of $FeTiO_3$ showing oxygens (blue), Fe (red) in the A layers, and Ti (black) ions in the B layers. In the solid solutions with Fe_2O_3 the Fe(III) ions enter both layers.

frustration of the interactions due to the difference in modulation lengths along the c axis, which results in a freezing event at a finite temperature T_f.[38–42] This magnetic partitioning was recently verified by low-temperature magnetization loops, which exhibited multiple metamagnetic transitions attributed to collective layer rotation.[65]

In order to investigate the intrinsic spontaneous magnetostriction and the magnetic frustration in this system, we recorded neutron diffraction patterns and magnetic susceptibility in a wide temperature range ($1.9\ \text{K} < T < 300\ \text{K}$) in the absence of a magnetic field. We found that below T_N the effects of thermal expansion disappear and that the antiferromagnetic ordering generates large spontaneous magnetostriction in $FeTiO_3$. First the results for the end-member ilmenite are presented and discussed based on phenomenological arguments, and then the results of the two solid solutions with 10 and 20 mol% hematite are discussed. The magnetic frustration in the two solid solutions is examined further based on zero-field-cooled and field-cooled magnetization curves, which exhibit magnetization self-reversal upon heating.

II. EXPERIMENTAL DETAILS

The end members $FeTiO_3$ (99.98%) and Fe_2O_3 (99.99%) were obtained as powders from Alpha Aesar (Germany). The solid solutions HI90 ($x = 0.9$) and HI80 ($x = 0.8$) were synthesized by solid oxide reaction at 1400 K in a radiation furnace for 48 hours sealed in a protective Ar atmosphere, and quenched in water. Magnetic ac susceptibility measurements were performed in a Quantum Design physical property measurement system (PPMS) between 2 K and 300 K at a frequency of 1 kHz and an amplitude of 1 Oe. The static dc magnetization was measured also in the PPMS under zero-field-cooled (ZFC) and field-cooled (FC) conditions between 2 K and 300 K. Neutron diffraction experiments on these samples were performed at the High Resolution Powder diffractometer for Thermal neutrons (HRPT)[66] at the Swiss Spallation Neutron Source (SINQ). Diffraction patterns were recorded at a wavelength of $\lambda = 1.8857$ Å in the temperature range between 1.9 K and 300 K in an Oxford Instruments vertical field cryomagnet. The powder samples (grain size $>100\ \mu$m) were kept in cylindrical vanadium sample holders during the experiments. The pattern acquisitions were performed at 1.9 K, 5 K, and 10 K; in 25 K steps between 25 K $\leqslant T \leqslant$ 150 K; and in 50 K steps between 150 K $\leqslant T \leqslant$ 300 K. The crystal and magnetic structure were refined by the Rietveld method using the Fullprof[67] software package.

III. RESULTS AND DISCUSSION

A. End-member ilmenite $FeTiO_3$

Figure 2 shows diffraction patterns of $FeTiO_3$ at (a) $T =$ 96 K and (b) $T = 1.9$ K. The refinement of the diffraction

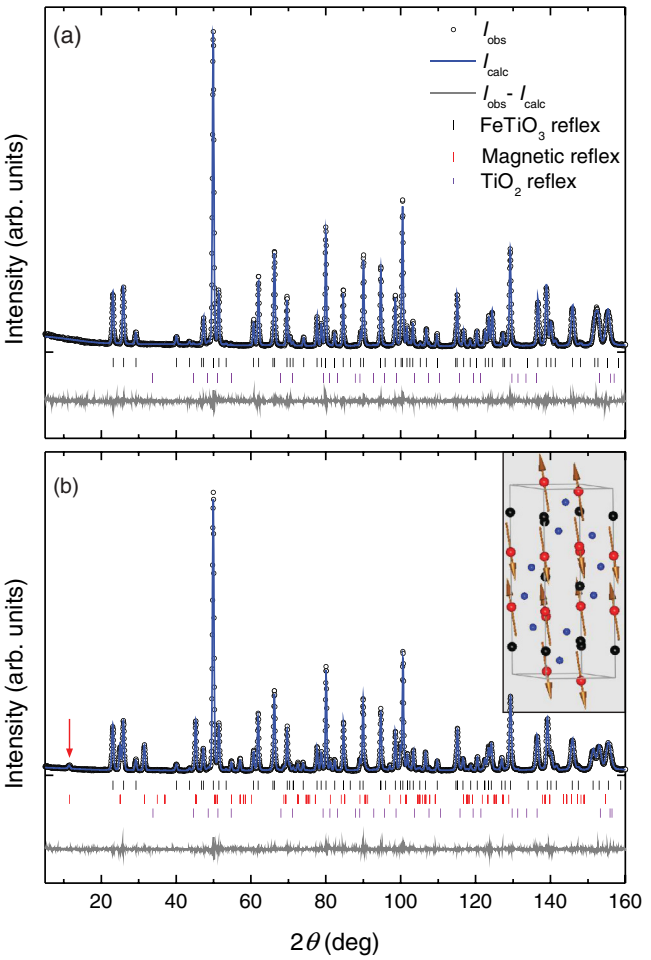

FIG. 2. (Color online) Powder neutron diffraction patterns of $FeTiO_3$ at (a) $T = 96$ K and (b) $T = 1.9$ K. Circles correspond to recorded intensities (I_{obs}); solid lines correspond to calculated patterns (I_{calc}); vertical bars indicate the Bragg-reflex positions of $FeTiO_3$, the magnetic order, and TiO_2; gray lines illustrate the difference between observed and calculated intensity ($I_{obs} - I_{calc}$). The inset in panel (b) illustrates the magnetic structure at $T = 1.9$ K. The arrow in (b) indicates the (0,0,3/2) reflection of the magnetic structure.

patterns fully confirms the accepted structure model of $FeTiO_3$, with Fe and Ti atoms located at the $6c$ $(0,0,z)$ sites with $z_{Fe} = 0.35498(5)$ and $z_{Ti} = 0.14692(5)$ at $T = 298$ K, and oxygen staying in the general $18f$ site with $\{x_O, y_O, z_O\} = \{0.31705(5), 0.02358(5), 0.24549(5)\}$. The strong difference in neutron scattering lengths between Fe and Ti (9.450×10^{-15} m for Fe and -3.438×10^{-15} m for Ti) allowed for a confident conclusion that the two metal sites are fully occupied by Fe and Ti, any cation disorder being excluded. The bond-valence sums calculation further confirms the oxidation states of $+2$ and $+4$ for Fe and Ti, respectively. The quality of the fits was monitored with the Rietveld profile factors R_p and the Bragg factors R_{Bragg}, which were on average around 4(1) and 2.0(5), respectively, thus confirming good fits, as can also be seen in Fig. 2 (see $I_{obs} - I_{calc}$ lines).

For temperatures $T > T_N$ only nuclear peaks were detectable, i.e., that of $FeTiO_3$, with negligible ($\approx$1 wt. %) impurity of rutile TiO_2. Upon cooling below the Néel temperature additional peaks appear [see Fig. 2(b)], which correspond to reflections of the commensurate magnetic structure in the ordered antiferromagnetic state. The magnetic reflections correspond to the propagation vector $\vec{k} = (0,0,3/2)$. The symmetry analysis of possible magnetic structures with this propagation vector [for the positions of Fe(II) ions in the $R\bar{3}$ symmetry] was carried out with the program SARAh-2k.[68] A total of six irreducible representations (IRs), for which the decomposition of the Fe(II) site has nonzero coefficients, enter the decomposition of the magnetic representation. All resulting possibilities were checked by Rietveld refinements, and it was found that a combination of the IRs Γ_1, with basis vector $\vec{\sigma}_1 = (0,0,3)$, and Γ_3, with basis vector $\vec{\sigma}_3 = (3,0,0)$, provides the best fit. This solution corresponds to an antiferromagnetic structure, in which the magnetic Fe(II) moments are parallel within the layers and antiparallel between adjacent layers. The inset to Fig. 2(b) shows a schematic of the magnetic ordering. The direction of the moment is predominantly along the c axis, with a smaller in-plane component. At $T = 1.9$ K, the projections of the magnetic moments are $4.381(2)\mu_B$ along the c axis and $0.567(2)\mu_B$ in the plane. The total magnetic moment of the Fe(II) cations amounts therefore to $4.417(4)\mu_B$, which is slightly higher than expected for the valence state of $+2$ ($3d^6$), since the theoretical ionic moment of Fe(II) in this configuration is 4.2 μ_B.[22] This suggests some orbital contributions to the total atomic magnetic moment.

At this point we note that the modeling of the magnetic structure was performed using the dipole approximation, i.e., assuming an isotropic magnetic form factor. In a recent work by Rotter and Boothroyd,[69] it has been shown that accounting for the anisotropic form-factor effects in $NdBa_2Cu_3O_{6+x}$, considering the $4f$ crystal field of the Nd ion, allowed for the correction of the previously accepted magnetic structure in that compound: A slight tilting of the Nd magnetic moments away from the c axis has been proven to be an artifact of the isotropic magnetic form-factor approximation used in the past.[70] Calculation of the magnetic form factor of Fe(II) using the McPhase program[71] revealed that the modeling of the magnetic structure can be considerably different when using the dipole approximation or the full approximation. The modeled magnetic intensity varies between the two approximations: The difference $(I_{full} - I_{dip})/I_{dip}$ is less than 5% for low angles ($2\theta < 60^\circ$) but becomes larger for higher angles [$(I_{full} - I_{dip})/I_{dip} > 20\%$]. One must consider, on the other hand, that the absolute magnetic intensity decreases with increasing diffraction angle, so that low-angle reflexes are more significant in the fitting process. With this in mind, we cannot definitely exclude the possibility that considering an anisotropic form factor for Fe(II) could improve the modeling of the magnetic structure in $FeTiO_3$.

Our neutron data, however, allow for the modeling of the magnetic structure in $FeTiO_3$, with an isotropic form factor, both with and without the small tilting of Fe magnetic moments away from the c axis. Our choice to describe the magnetic structure with this tilting is based on three arguments: (i) We find the (0,0,3/2) magnetic reflex [see arrow in Fig. 2(b)] which can only exist if there is an a axis component of the Fe magnetic moment;[72] (ii) we obtain a better R factor for the magnetic phase in our refinement if we allow for the tilting [$R_{mag} = 6.2(1)$ vs $R_{mag} = 7.1(1)$ for the model without tilting]; and (iii) the tilting of the magnetic moments in $FeTiO_3$ has been established in detailed earlier works on single crystals.[72,73]

Figure 3 shows the evolution of the unit cell volume and the individual axes with decreasing temperature. Upon cooling from room temperature, both a and c axes decrease due to the reduction of thermal agitation. Between 200 K $\leqslant T \leqslant$ 300 K both axes, and in turn the unit cell volume, decrease linearly with temperature. Between 200 K and 100 K the curve for the c axis flattens with a weak minimum at 150 K. Upon further cooling the length of the c axis increases, and upon crossing the Néel temperature, the rate of increase is enhanced drastically. The length of the c axis at $T = 1.9$ K is 14.1054(2) Å, which is 0.116% higher than the value at room temperature. The lateral dimensions (a axis) reveal a nearly linear decrease with temperature, with a kink at T_N. The overall reduction of the a axis dimension is 0.248%. The volume of the unit cell also exhibits a linear decrease between 200 K and 300 K and below 150 K it describes a parabolic-like behavior, with a saturation below T_N, where it stays approximately constant within the error bar. Apparently, the effects of thermal expansion disappear below T_N.

The change of the cell axes is obviously associated with the antiferromagnetic ordering at T_N. Due to the intrinsic nature of this effect, we cannot measure the unit cell dimensions in the absence of magnetic order at low temperature. We can, however, extrapolate the linear region between 200 K and 300 K to estimate the dimensions at low temperature and thus the spontaneous magnetostriction coefficients, i.e., the magnetic contributions to the thermal expansion $(\Delta l/l)_{mag}$. In doing this, we consider thermodynamic saturation effects, which require that the order parameter Q saturates as $T \to 0$.[74,75] This means that the cell dimensions, which are coupled to the order parameter, should be constant at low temperature, and follow a trend described by[76]

$$l(T) = l(0) + \alpha\theta_S \coth(\theta_S/T), \quad (1)$$

where $l(T)$ is the lattice parameter at temperature T, $l(0)$ is the zero-temperature lattice parameter, θ_S is the saturation temperature, and α is a scaling prefactor. We perform the extrapolation procedure by initially assuming that the spontaneous volume strain is negligible. We therefore fit the volume vs temperature

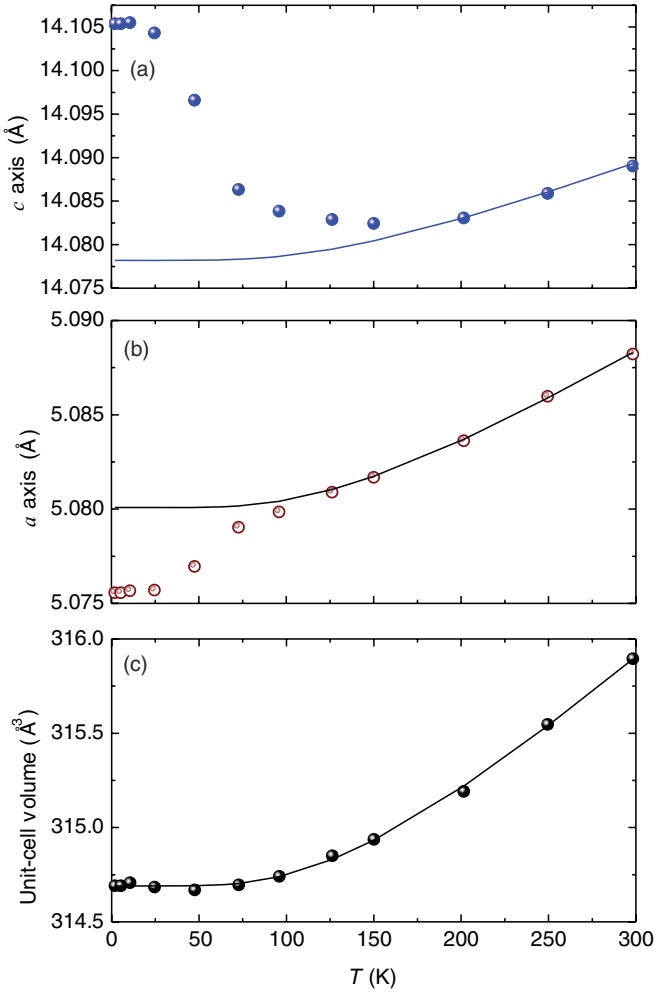

FIG. 3. (Color online) Temperature dependencies of (a) the c axis, (b) the a axis, and (c) the unit-cell volume. Errors are smaller than the symbol size. The solid lines are extrapolations to low temperature using Eq. (1).

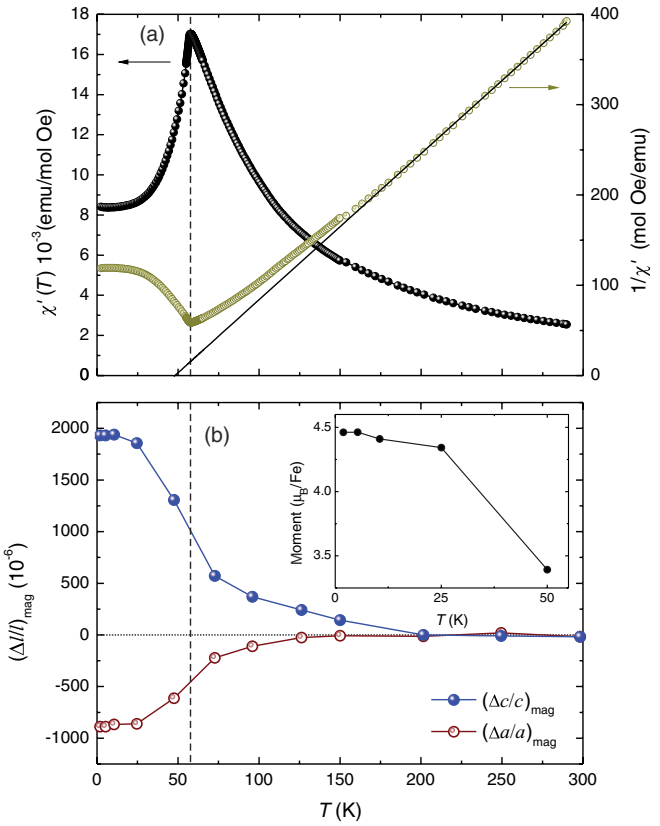

FIG. 4. (Color online) (a) Magnetic susceptibility of $FeTiO_3$ as a function of temperature (left ordinate) and inverse susceptibility (right ordinate). (b) Magnetostriction coefficients as a function of temperature. Solid spheres correspond to the c axis coefficient $[(\Delta c/c)_{\rm mag}]$ and open spheres to the a axis coefficient $[(\Delta a/a)_{\rm mag}]$. The inset to (b) shows the magnetic moment per Fe(II) ion at each temperature. The dashed line in both panels indicates the location of $T_{\rm N}$.

curve and determine the saturation temperature, which for the end-member ilmenite is $\theta_S = 210(10)$ K. We then fix this value and fit the cell axes by adjusting the scale parameter α and the initial value $l(0)$. The extrapolation curves can be seen in Fig. 3.

We define the c-axis coefficient as $(\Delta c/c)_{\rm mag} = [c_{\rm AFM}(T) - c_{\rm PM}(T)]/c_{\rm PM}(T)$ and the a-axis coefficient as $(\Delta a/a)_{\rm mag} = [a_{\rm AFM}(T) - a_{\rm PM}(T)]/a_{\rm PM}(T)$ at each temperature. The index AFM corresponds to the antiferromagnetic state (measured) and the index PM to the paramagnetic state (estimated by extrapolation) for both axes. All coefficients are given in units of microstrains, i.e., parts per million (ppm).

The comparison between magnetic ordering and magnetostriction is demonstrated in Fig. 4. Panel (a) in the figure shows the in-phase susceptibility and the inverse susceptibility of $FeTiO_3$ as a function of temperature. The susceptibility increases steadily with decreasing temperature, and at $T_{\rm N}$ it exhibits a peak. Below $T_{\rm N}$ it decreases again due to the onset of anisotropy in the antiferromagnetic structure, and at low temperature it reaches a plateau, which comes from contributions of crystallites with their c axis perpendicular to the measurement axis.[23] The inverse susceptibility is linear at high temperature ($T > 150$ K), due to the absence of interactions in that regime, and reveals a Weiss constant of $\Theta = 49(2)$ K. At around 150 K, however, it departs from linearity, indicating the onset of fluctuations of the atomic magnetic moments.

As seen in Fig. 4(b), which shows the magnetostriction coefficients as a function of temperature, the onset of magnetic fluctuations [i.e., the departure from linearity in $1/\chi(T)$] marks the appearance of the spontaneous magnetostriction. Then, with decreasing temperature, as the fluctuations become stronger upon approaching the magnetic ordering transition, $(\Delta c/c)_{\rm mag}$ increases markedly to 500(100) ppm whereas $(\Delta a/a)_{\rm mag}$ is negative and reaches $-250(100)$ ppm. Upon crossing $T_{\rm N}$ and entering the magnetically ordered phase, $(\Delta c/c)_{\rm mag}$ jumps to 1300(100) ppm and keeps increasing with decreasing temperature, reaching 1950(100) ppm at 1.9 K. In contrast, $(\Delta a/a)_{\rm mag}$ reaches $-600(100)$ ppm upon ordering and only reaches $-900(100)$ ppm at low temperature. The errors given in parentheses are estimates, based on the extrapolation from the 200–300 K interval down to 0 K. Within the error bar of $(\Delta c/c)_{\rm mag}$, this is, to our knowledge, the highest spontaneous magnetostriction for an antiferromagnetic oxide.

The above observations allow for a phenomenological interpretation, without the need for extensive theoretical

argumentation. The fact that spontaneous magnetostriction appears in the temperature regime where magnetic moment fluctuations start ($T_N < T < 150$ K) indicates that the dimension changes are due to magnetic contributions. With this in mind, we consider two scenarios: (i) The onset of magnetic order changes the spin-orbit coupling, which then enhances the Fe(II)-Ti(IV) separation along the c axis upon ordering,[22] and (ii) the enhancement of the magnetic exchange interactions gives rise to exchange striction,[79] where inter-ionic distances are changed in order to lower the interaction energy.[2] The possibility of charge-transfer-induced spacing variations[80] can be dismissed, since the valence state of A sites was found to be +2. Moreover, crystal-field striction effects can be neglected because they are not associated with long-range order.[2]

The first scenario suggests a spin-orbit-coupling-induced mechanism that changes with temperature and follows the trend of the order parameter Q, because the order parameter is coupled to the strain.[77] The second scenario suggests a rather continuous change with temperature, as exchange interactions become stronger with decreasing thermal energy. We argue that both effects contribute to the observed behavior. Upon antiferromagnetic ordering at T_N, the exchange interactions are dominant and the energy of the interactions depends on the inter-ion distances. The spontaneous strain observed here stems therefore from the minimization of the interaction energy via adjustment of the distances, i.e., giving rise to exchange striction.[2,81] The antiparallel alignment of the magnetic moments between Fe layers is enforced by the weak but long-range dipole-dipole interactions. Below T_N, with decreasing temperature, the interactions and the magnetic moment become stronger and cause a further increase in $(\Delta c/c)_{mag}$. This can be verified by comparing the course of $(\Delta c/c)_{mag}$ to the course of the magnetic moment m [see inset to Fig. 4(b)], as extracted from the neutron data. These findings are in excellent agreement with the predictions of exchange-striction theory with two-ion interactions, which predict lattice distortions in antiferromagnetic systems.[2]

Exchange striction does not predict spontaneous magnetostriction at temperatures above T_N, as we observe here. We suggest, however, that the presence of spontaneous strain above T_N in ilmenite originates from short-range interactions which are evident above T_N as seen in the nonlinearity of the inverse susceptibility. This effect was also observed in $R_2Fe_{17}C_x$ (R = Y and Tb),[5] and Lu_2Fe_{17},[78] to a lesser degree.

B. Solid solutions with 10% and 20% Fe_2O_3

Similar to the discussion of the end-member ilmenite, the investigation of the magnetostrictive properties of Fe(III)-doped ilmenite (hemo-ilmenite) begins with neutron diffraction experiments in a wide temperature range. Figure 5 shows an example at $T = 1.9$ K for samples HI90 and HI80. Rietveld refinement of the cation site occupancies confirms the chemical compositions of HI90 and HI80 with 10(1)% and 20(1)% Fe at the B sites, respectively. In addition to the changing composition in each sample, a shifting of the site positions in the unit cell was found. This, in turn, marks the change in layer spacing with different cation composition. In the end-member ilmenite the Fe-Ti distance, i.e., the distance between the 6c (0,0,z) cation sites, was 0.20806(5) uc (uc = unit cell

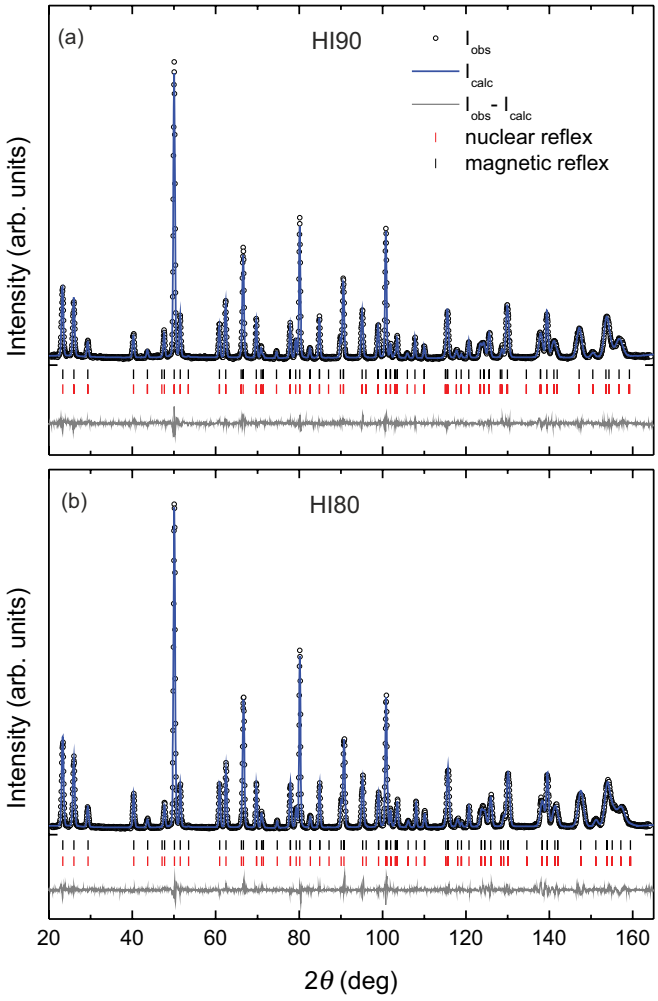

FIG. 5. (Color online) Neutron diffraction of (a) HI90 and (b) HI80 at $T = 1.9$ K. Circles correspond to the observed intensity I_{obs}; blue solid lines correspond to calculated patterns I_{calc}; gray lines correspond to the deviation $I_{obs} - I_{calc}$; black vertical bars correspond to the locations of the nuclear Bragg reflections, and red vertical bars correspond to the magnetic reflections.

dimensions). In the HI90 sample we find a significant reduction of 1% to 0.20689(5) uc, and in HI80 a further reduction of 2% to 0.20357(5) at $T = 298$ K. While in the $R\bar{3}$ symmetry the Fe(II) and Ti(IV) are partitioned into consecutive layers, the Fe(III) enters all layers. This leads to a distortion of the O octahedra around Fe(III) because of charge imbalances; i.e., the Fe(III) cation pulls the O ions closer to share more charge than the neighbors. Considering that consecutive layers share the faces and corners of the octahedra, the layers are pulled closer together with increasing Fe(III) contents. This is also demonstrated in the changes of the cell axes with increasing Fe(III) contents: The lateral dimension of the unit cell (a axis) exhibits a small reduction at each compositional step (0.05–0.1 %), while the c axis changes more (0.1–0.5 %). At $T = 298$ K the cell dimensions are $a = 5.08166(5)$ Å and $c = 14.01308(5)$ Å for HI90, and $a = 5.07927(5)$ Å and $c = 13.99315(5)$ Å for HI80.

In contrast to the diffraction patterns of the end-member ilmenite, no additional peaks appear upon the onset of

magnetic order. A pronounced increase in intensity, however, is clearly due to magnetic reflections in the material. This means that the magnetic peaks are in exactly the same positions as the nuclear peaks, which in turn means that the magnetic unit cell is identical to the crystal unit cell. With decreasing temperature, the magnetic intensity increases and becomes maximum at the lowest recorded temperature. The strongest magnetic reflections lie in the low-angle region and the strongest peaks are the (003) and (101) reflexes (at $2\theta = 23.30^\circ$ and 25.99°).

The magnetic reflections correspond to the propagation vector $\vec{k} = (0,0,0)$; i.e., the magnetic unit cell is identical to the structure unit cell. The symmetry analysis of the possible magnetic structures was performed again with the program SARAh-2k. In this case, two atoms were used in the magnetic unit cell, i.e., one Fe ion at the A site and one at the B site, with the occupancy at the B site adjusted to the extracted site occupancy (10% for HI90 and 20% for HI80). The symmetry analysis results in the same six IRs, as in ilmenite. Rietveld refinement with different IRs was performed, and it was found that the magnetic intensity can be fitted with various spin configurations. The fact that the only degree of freedom in this fitting procedure is the additional intensity of the peaks hinders the exact determination of the magnetic structure in hemo-ilmenite. Considering that two basis functions are needed for the two atoms, four fit parameters are adjusted during the refinement. Moreover, certain peaks can be fitted with both basis function contributions; i.e., they are complementary. Therefore, only qualitative arguments can be made, based on these neutron data.

For a direct comparison with the end-member ilmenite, the same IRs were used in the final refinement, i.e., Γ_1 $[\vec{\sigma}_1 = (0,0,3)]$ and Γ_3 $[\vec{\sigma}_1 = (3,0,0)]$. Although the results after each Rietveld refinement show strong deviations (angles and magnitudes of the magnetic moments vary), it allows a remarkable observation: The magnetic moments lie predominantly inside the layer, with a small component along the c axis. The doping of ilmenite with Fe(III) causes a declination of the moments along the basal plane. This is a surprising observation, considering the findings of Ishikawa *et al.*[39] and Arai *et al.*[40] also based on neutron experiments and susceptibility experiments with single crystals.[38] Recent studies by Robinson *et al.*[62] and Harrison *et al.*[82] assumed that the magnetic moment lies inside the basal plane, but mostly in end-member exsolution lamellae. Therefore, our observation establishes the fact that even within the error interval of the magnetic refinements, the magnetic moment lies predominantly inside the layers at low temperature. The same refinement routine was used for all temperatures, and it was found that the angles of the magnetic moments change: With increasing temperature there is a tendency to turn towards the c axis.

At the lowest temperature ($T = 1.7$ K), an external magnetic field of 20 kOe was applied to the samples and removed. Then, neutron diffraction patterns were recorded with the same temperature steps, as upon cooling. With switching on the field, a significant number of the powder grains turned towards the field, thus inducing a preferred orientation in the total sample. This provided a further difficulty in refining the neutron data, especially for the magnetic intensity. The unit cell dimensions, however, could still be extracted with very good accuracy because the preferred orientation only affects the relative intensity of the reflexes, not their location.

Figures 6(a)–6(c) show the unit cell dimensions in the HI90 sample, upon cooling and upon heating the sample, after application of the field. As seen in this figure, upon cooling both dimensions, i.e., the c and the a axis, decrease due to decreasing thermal agitation in the lattice. Upon crossing the Curie temperature, a departure from linearity is observed, and at low temperature $T < 50$ K, the a axis remains approximately constant, whereas the c axis increases slightly. The unit cell volume exhibits a similar behavior to the one of ilmenite, which is parabolic-like and below $T = 50$ K it is approximately constant. After application of the external field, the unit cell dimensions are changed at low temperature and the curve exhibits a hysteresis. The hysteresis decreases with increasing temperature, and at $T = 25$ K the heating and the cooling curves are identical.

The results for the HI80 sample are quite similar, as seen in Figs. 6(d)–6(f). The main difference in this composition is that the c axis exhibits an almost linear behavior with the temperature and shows no pronounced increase at low temperature, as is the case in HI90. The behavior of the a axis upon cooling also changes and shows an enhanced parabolic-like curvature with temperature; the same trend is also seen for the overall unit cell volume. After the application of the external field the situation is again similar to the one observed for HI90: A thermal hysteresis is seen, which decreases with increasing temperature. It does not fully disappear at $T = 25$ K, as in HI90, but somewhere between 25 K and 50 K. Above that temperature, the curves are again identical and increase with increasing temperature.

The change of lattice dimensions upon magnetic ordering should be expected, as was observed in the end-member ilmenite, which exhibited large spontaneous magnetostriction. However, the observation of the thermal hysteresis in both samples provides an insight into the magnetostrictive effects in hemo-ilmenite solid solutions. Considering that in the low-temperature regime ($T < 25$ K) the system exhibits a spin-glass-like freezing,[38,39] the hysteretic effects are directly associated with the freezing transition. An external magnetic field can break the symmetry of a spin glass and induce a transition from a non-ergodic state to an ordered state.[83] Although in this case there is no spin glass, as inferred from the long-range magnetic order indicated by the neutron data, the field induces a change in the configuration of the magnetic structure.[42,65] Therefore, the new magnetic configuration involves different exchange-energy balance schemes, which alter the ionic spacings accordingly. The reduction in both dimensions suggests that the system switches from generally antiparallel to parallel configuration, considering that antiparallel configuration (as in ilmenite) causes elongation of the c axis.

In order to extract the spontaneous magnetostriction coefficients, the same approach was taken, as with ilmenite. First the volume was fitted using Eq. (1) and a saturation temperature of $\theta_S = 145(5)$ K for both solid solutions was found. The extrapolation function was then scaled to the cell axes, while keeping θ_S fixed. The extrapolated values were

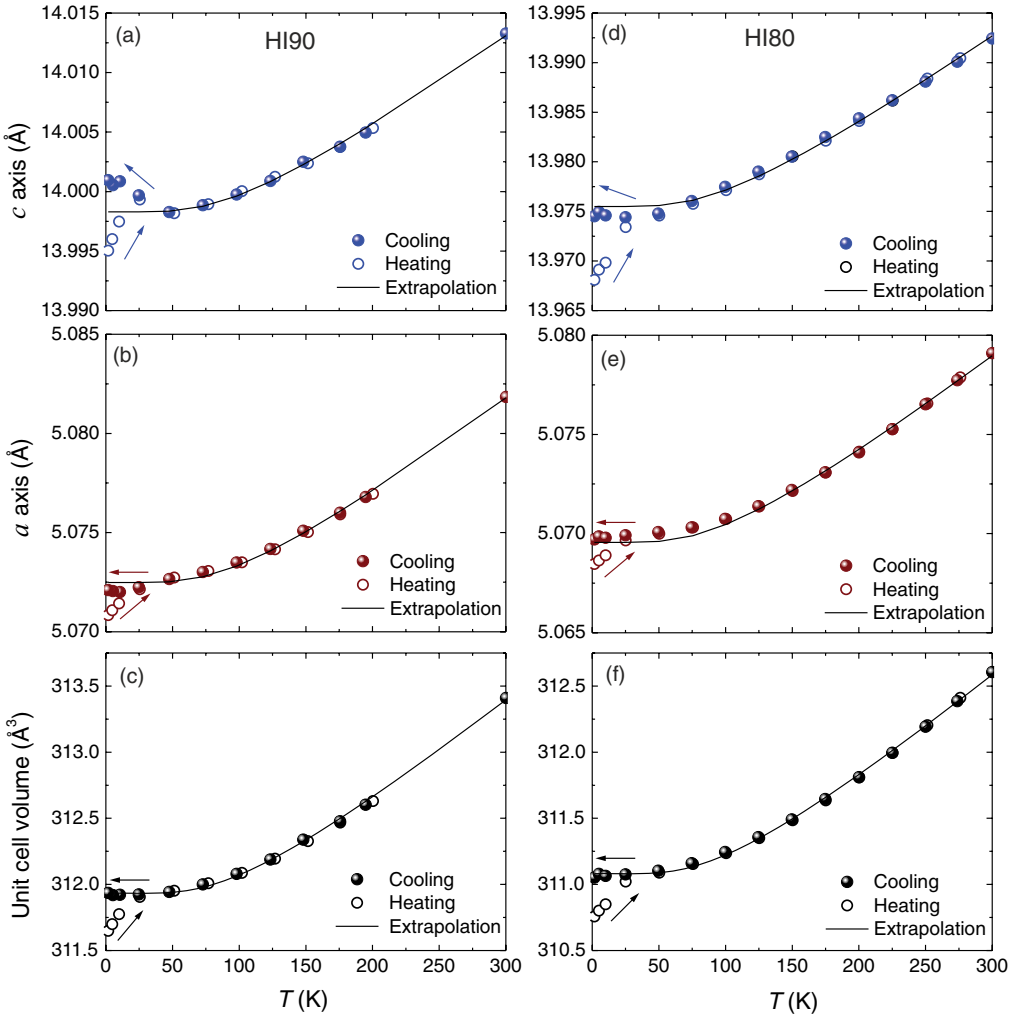

FIG. 6. (Color online) Unit cell dimensions in HI90 (left) and HI80 (right) as a function of temperature, as extracted from the neutron data. Top panels show the c axis, middle panels show the a axis, and bottom panels show the unit cell volume of each compound upon cooling and heating. Errors are smaller than the symbol size. The solid lines are extrapolations using Eq. (1).

used as a reference to estimate $(\Delta c/c)_{\mathrm{mag}}$ and $(\Delta a/a)_{\mathrm{mag}}$. The results for both samples are shown in Fig. 7.

As seen in the figure, spontaneous magnetostriction is practically zero for both compounds upon cooling through their respective Curie temperature [150(1) K for HI90 and 235(1) K for HI80]. At the lowest temperature, small values in the range of 100–200 ppm are obtained. In general, the spontaneous magnetostriction of both compounds is negligible, compared to the one of the end-member ilmenite. This is probably due to two reasons: The spin-configuration and thus the exchange interactions are strongly changed, and the Fe(III) doping changes the charge balance inside the planes and along subsequent planes, which in turn changes the bond strengths and their competition with the exchange interactions. This means that the change in bond strength can inhibit the adjustment of inter-ion distances and thus reduce the energy of the exchange interactions.

After the application of the external field, however, a strong change is observed, where the spontaneous magnetostriction on both axes assumes significant negative values in both solid solutions. This directly indicates that the configuration change induced by the external field has a strong impact on the projections of the magnetic moments along the a and c axes, and in turn of the exchange interactions.

In conclusion, the neutron data reveal that the solid solutions with compositions $x = 0.9$ and 0.8 exhibit long-range magnetic order even at low temperatures. This contradicts previous interpretations of a spin-glass state at low temperature.[39] Moreover, the results show that with increasing Fe(III) doping of the $FeTiO_3$ structure the magnetic moments depart from the c axis and become more tilted towards the a axis of the unit cell. The spontaneous magnetostriction is greatly reduced in the solid solutions, compared to the large values for the end-member ilmenite.

In order to better understand the field-induced lattice change in HI90 and HI80 at low temperature, we performed ac susceptibility and dc magnetization experiments. Initially, the ac susceptibility was measured in detail to find the exact Curie temperature of the two compounds HI90 and HI80.

Figure 8 shows the in-phase (top panels) and out-of-phase (bottom panels) susceptibilities of both samples. As seen in the figure, both solid solutions exhibit a well-pronounced

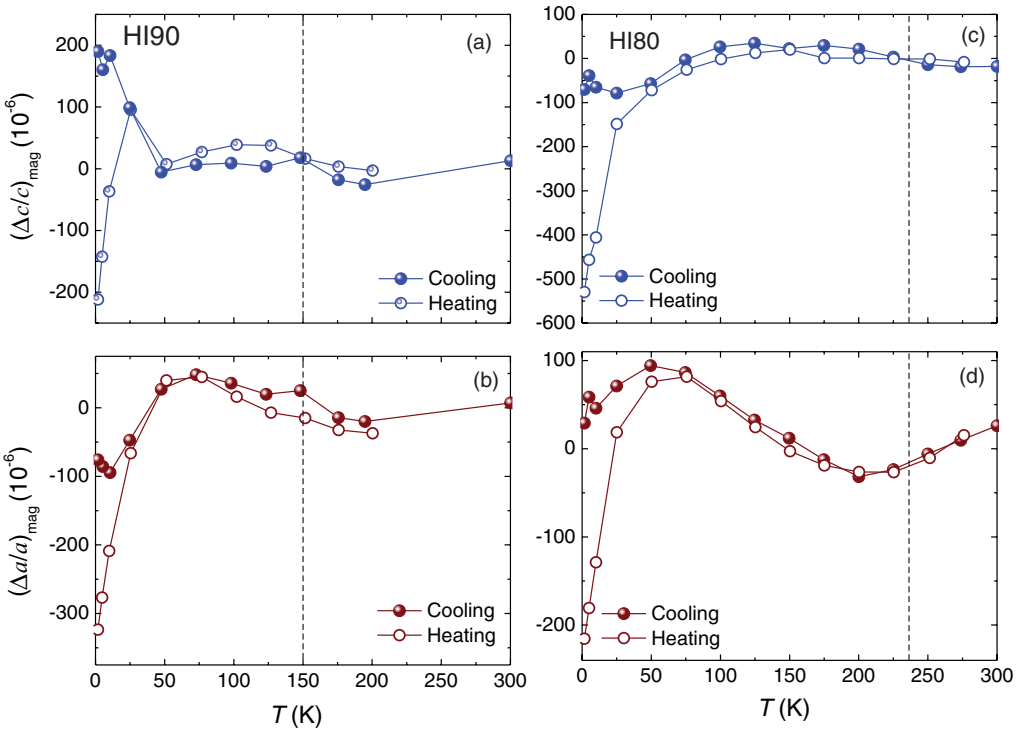

FIG. 7. (Color online) Spontaneous magnetostriction coefficients of HI90 [(a), (b)] and HI80 [(c), (d)] between 2 K and 300 K upon cooling and heating. Top panels show $(\Delta c/c)_{\mathrm{mag}}$ and bottom panels show $(\Delta a/a)_{\mathrm{mag}}$. The vertical dashed lines show the location of the Curie temperature for each sample, as determined from ac susceptibility measurements (see Fig. 8).

sharp ordering at their respective Curie temperature T_{C}. The exact location of the transition at T_{C} is found at the onset of $\chi''(T)$ upon cooling, as indicated in the figure by arrows. The values for T_{C} were 150(1) K for HI90 and 235(1) K for HI80. The values of T_{C} are in good agreement with the respective compositions according to the well-known phase diagrams.[36,37] The onset of hysteretic effects is very abrupt, unlike the behavior of χ'. The in-phase component of

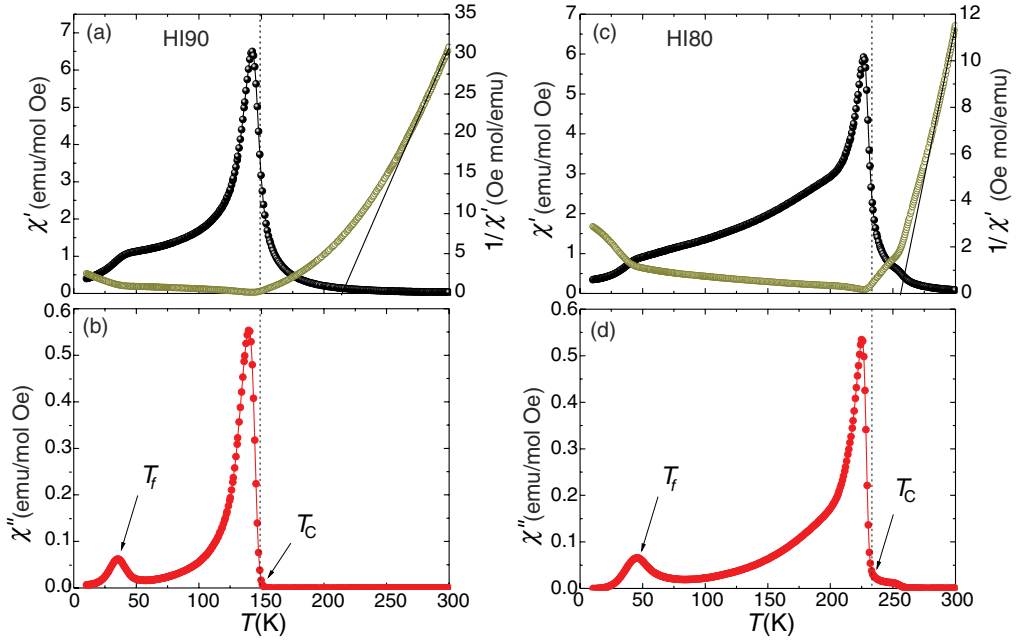

FIG. 8. (Color online) Magnetic ac susceptibility of HI90 [(a), (b)] and HI80 [(c), (d)] between 2 K $\leqslant T \leqslant$ 300 K. Top panels show the in-phase component χ' (left ordinate) and the inverse susceptibility $1/\chi'$ (right ordinate). Bottom panels show the out-of-phase component of the susceptibility χ''. The arrows in the bottom panels indicate the location of the Curie temperature T_{C} and the freezing temperature T_{f}. The measurements were performed at a frequency of 1 kHz and an amplitude of $H_{ac} = 1$ Oe.

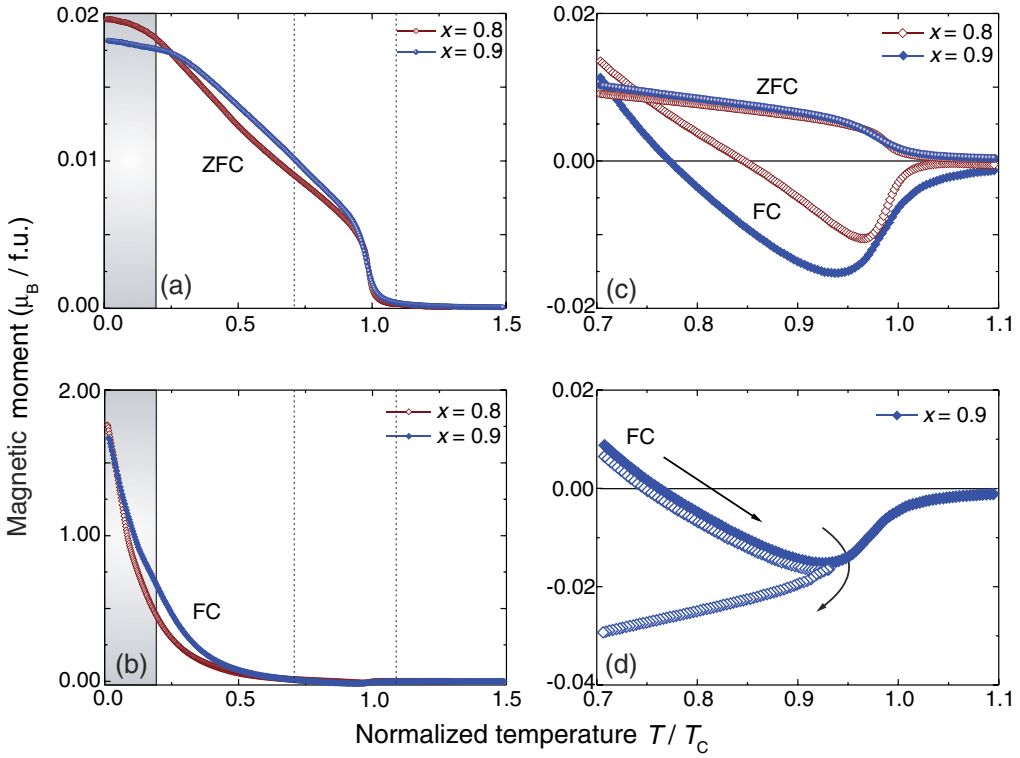

FIG. 9. (Color online) Measured magnetization curves for HI90 ($x = 0.9$) and HI80 ($x = 0.8$). (a) Magnetic moment using no bias field (ZFC). (b) Magnetic moment of the same compounds after having field cooled (FC) to 2 K using a field of 10 kOe. (c) Detailed view of (a) and (b) in the range $0.7 < T/T_C < 1.1$, and (d) repetition of the measurement with reversed direction after magnetization self-reversal. The arrows indicate the direction of the measurement. The temperature is normalized to the respective Curie temperature, and the shaded region in (a) and (b) indicates the $T < T_f$ regime.

the susceptibility increases strongly before the transition and exhibits a sharp Hopkinson peak just below the transition. With decreasing temperature χ' decreases gradually and exhibits an enhanced decrease close to 50 K. The high-temperature linear expansion was fitted with the Curie-Weiss law, and is also shown in the figures. The inverse susceptibility obeys a linear law between 270 K and 300 K. In the HI90 sample, the inverse susceptibility departs from linearity at around 270(10) K, and in the HI80 sample at around 280(10) K. The Weiss constants are $\Theta = 215(5)$ K for HI90 and 255(5) K for HI80. For HI90, Θ is much higher than the actual ordering temperature. For HI80, however, Θ is quite close to the actual T_C and does not suggest significant correlations above the ordering transition.

Below the ordering transition, χ'' decreases strongly with decreasing temperature and exhibits a well-pronounced peak below $T = 50$ K for both solid solutions. This peak arises due to dissipation effects during the spin-glass-like freezing of the magnetic configuration.[28,38,39,41,42] As seen from the neutron data, however, this freezing transition does not constitute a spin-glass transition, but a change in layer configuration in the system. Since the change in layer configuration is collective, the effect will also be detectable in the total magnetization of the system. Therefore we measured the net magnetization between 2 K and 300 K under ZFC and FC conditions.

First, we performed zero-field-cooling of the system down to 2 K and measured the magnetization upon heating to 300 K without using any bias field. The resulting curve exhibits typical ferrimagnetic behavior in both samples, with a decrease in the magnetic moment with increasing temperature and a disappearance at the Curie temperature T_C [see Fig. 9(a)]. We then cooled the system down to 2 K again, but this time under FC conditions with $H_{cool} = 10$ kOe. We switched off the field at 2 K and measured the magnetization upon heating. The resulting curve changes drastically compared to the ZFC curve [Fig. 9(b)]: The net moment at 2 K is about two orders of magnitude higher, and with increasing temperature the moment exhibits exponential decay in the vicinity of the freezing temperature T_f. This striking increase of the magnetic moment reflects the modified layer configuration induced by the external field, as seen in the neutron diffraction data, which suggested parallel alignment of the Fe-rich layers. Upon approaching the Curie temperature an unexpected reversal occurs and the magnetic moment crosses to negative values before it vanishes [Fig. 9(c)]. Moreover, the ZFC curve, for which the samples were magnetized at 2 K with 10 kOe, becomes identical to those obtained under FC conditions. This behavior corresponds to the previously reported symmetry breaking in this system at low temperatures.[42]

The form of the FC curve depends on the bias field. For cooling fields less than 5 kOe, no magnetization reversal occurs (data not shown). This is because the field has to be strong enough to overcome a certain energy barrier in order to induce the layer configuration of the FC thermodynamic behavior of the curve in Fig. 9(b).

In order to test the reversibility of the reversal of the FC behavior of $H_{cool} > 5$ kOe, we repeated the field-cooled

measurement, but stopped after the reversal, at $T/T_C = 0.9$. Then we started measuring the moment upon cooling. As seen in Fig. 9(d), the magnetization does not return to positive values, and the net moment increases in the negative direction with decreasing temperature. In fact, this curve is a reflection of the unbiased ZFC curve seen in Fig. 9(a), which shows typical ferrimagnetic behavior, but on the negative side of the axis. This means that the system is in the same energetic state, which is degenerate with respect to positive-negative symmetry in the absence of an external field.

IV. CONCLUSIONS

In conclusion, we have shown that ilmenite exhibits large spontaneous magnetostriction below the ordering temperature of 58 K, where the c axis of the unit cell grows strongly with decreasing temperature. This is attributed to exchange interactions between the Fe-rich layers, which need to adjust their distance to reduce the energy. For the hemo-ilmenite solid solutions with $x = 0.9$ and 0.8, it was found that with increasing Fe(III) content the spins tend to tilt towards the basal planes, i.e., away from the c axis. This is reflected in the vanishing of the spontaneous magnetostriction in both compounds. This strong change is attributed to the change in symmetry of exchange interactions due to the presence of Fe(III). By applying an external field we could modify the layer configuration in the Fe-doped ilmenites and generate a parallel alignment of Fe-rich layers. This generates a strong increase in the net magnetic moment and a reduction of the unit cell dimensions.

ACKNOWLEDGMENTS

The authors would like to thank E. Fischer for his assistance in the sample preparation process, and R. J. Harrison for fruitful discussions. We thank M. Rotter for calculations with the McPhase program and discussions regarding the modeling of the magnetic structure in our samples. This work is partly based on the results of experiments carried out at the Swiss Spallation Neutron Source SINQ, Paul Scherrer Institute, Villigen, Switzerland. It was funded by the Swiss National Science Foundation via Grant No. 200021-121844.

*Corresponding author; michalis.charilaou@erdw.ethz.ch

[1] E. Du Trempolet de Lacheisserie, *Magnetostriction: Theory and Application of Magnetoelasticity* (CRC Press, Boca Raton, FL, 1993).
[2] M. Doerr, M. Rotter, and A. Lindbaum, Adv. Phys. **54**, 1 (2005).
[3] E. F. Wassermann, in *Handbook of Magnetic Materials*, edited by K. H. J. Bushow and E. P. Wohlfarth, Vol. 5 (Elsevier Science, 1990), Chap. 3.
[4] M. Shiga and Y. Nakamura, J. Phys. Soc. Jpn. **26**, 24 (1969).
[5] A. V. Andreev, F. R. de Boer, T. H. Jacobs, and K. H. J. Buschow, Physica B **175**, 361 (1991).
[6] Z. W. Ouyang, G. H. Rao, H. F. Yang, W. F. Liu, G. Y. Liu, X. M. Feng, and J. K. Liang, J. All. Comp. **372**, 76 (2004).
[7] J. Hemberger, T. Rudolf, H.-A. Krug von Nidda, F. Mayr, A. Pimenov, V. Tsurkan, and A. Loidl, Phys. Rev. Lett. **97**, 087204 (2006).
[8] J. Hemberger, H.-A. Krug von Nidda, V. Tsurkan, and A. Loidl, Phys. Rev. Lett. **98**, 147203 (2007).
[9] X. G. Zheng, H. Kubozono, H. Yamada, K. Kato, Y. Ishiwata, and C. N. Xu, Nat. Nanotechnol. **3**, 724 (2008).
[10] P. Morin and D. Schmitt, in *Ferromagnetic Materials*, edited by K. H. J. Buschow and E. P. Wohlfarth, Vol. 5 (Elsevier Science, 1990).
[11] I. D. Mayergoyz, *Handbook of Giant Magnetostrictive Materials* (Academic Press, San Diego, 2000).
[12] C. Detlefs, A. H. M. Z. Islam, T. Gu, A. I. Goldman, C. Stassis, P. C. Canfield, J. P. Hill, and T. Vogt, Phys. Rev. B **56**, 7843 (1997).
[13] C. Song, Z. Islam, L. Lottermoser, A. I. Goldman, P. C. Canfield, and C. Detlefs, Phys. Rev. B **60**, 6223 (1999).
[14] V. L. Moruzzi, Phys. Rev. B **41**, 6939 (1990).
[15] H. Akai and P. H. Dederichs, Phys. Rev. B **47**, 8739 (1993).
[16] M. van Schilfgaarde, I. A. Abrikosov, and B. Johansson, Nature (London) **400**, 46 (1999).
[17] V. Crisan, P. Entel, H. Ebert, H. Akai, D. D. Johnson, and J. B. Staunton, Phys. Rev. B **66**, 014416 (2002).
[18] S. Khmelevskyi and P. Mohn, Phys. Rev. B **66**, 220404(R) (2002).
[19] S. Khmelevskyi, I. Turek, and P. Mohn, Phys. Rev. Lett. **91**, 037201 (2003).
[20] S. Khmelevskyi and P. Mohn, Phys. Rev. B **69**, 140404(R) (2004).
[21] A. V. Ruban, S. Khmelevskyi, P. Mohn, and B. Johansson, Phys. Rev. B **76**, 014420 (2007).
[22] J. B. Goodenough and J. Stickler, Phys. Rev. **164**, 768 (1967).
[23] H. Kato, M. Yamada, H. Yamauchi, H. Hiroyoshi, H. Takei, and H. Watanabe, J. Phys. Soc. Jpn. **51**, 1769 (1982).
[24] H. Kato, S. Funahashi, Y. Yamaguchi, M. Yamada, and H. Takei, J. Magn. Magn. Mater. **31–34**, 617 (1983).
[25] H. Kato and Y. Nakagawa, Physica B **201**, 80 (1994).
[26] T. Varga *et al.*, Phys. Rev. Lett. **103**, 047601 (2009).
[27] R. J. Harrison and S. A. T. Redfern, Phys. Chem. Miner. **28**, 399 (2001).
[28] A. U. Gehring, H. Fischer, E. Schill, J. Granwehr, and J. Luster, Geophys. J. Int. **169**, 917 (2007).
[29] M. Charilaou, J. F. Löffler, and A. U. Gehring, Phys. Chem. Miner. **32**, 87 (2012).
[30] R. A. Wright, F. H. Cocks, D. T. Vaniman, R. D. Blake, and T. T. Meek, J. Mater. Sci. **24**, 1337 (1989).
[31] Y. J. Kim, B. Gao, S. Y. Han, M. H. Jung, A. K. Chakraborty, T. Ko, C. Lee, and W. I. Lee, J. Phys. Chem. C **113**, 19179 (2009).
[32] D. S. Ginley and M. A. Butler, J. Appl. Phys. **48**, 2019 (1977).
[33] D. Sherman, Phys. Chem. Miner. **14**, 355 (1987).
[34] R. J. Harrison, S. A. T. Redfern, and R. I. Smith, Am. Mineral. **85**, 194 (2000).
[35] R. J. Harrison, U. Becker, and S. A. T. Redfern, Am. Mineral. **85**, 1694 (2000).
[36] N. Brown, A. Navrotsky, G. L. Nord, Jr., and S. K. Banerjee, Am. Mineral. **78**, 941 (1993).
[37] R. Engelmann, A. Kontny, and D. Lattard, J. Geophys. Res. **115**, B12107 (2010).
[38] Y. Ishikawa, M. Arai, N. Saito, M. Kohgi, and H. Takei, J. Magn. Magn. Mater. **31–34**, 1381 (1983).

[39]Y. Ishikawa, N. Saito, M. Arai, Y. Watanabe, and H. Takei, J. Phys. Soc. Jpn. **54**, 312 (1985).
[40]M. Arai, Y. Ishikawa, N. Saito, and H. Takei, J. Phys. Soc. Jpn. **54**, 781 (1985).
[41]A. U. Gehring, G. Mastrogiacomo, H. Fischer, P. D. Weidler, E. Müller, and J. Luster, J. Magn. Magn. Mater. **320**, 3307 (2008).
[42]M. Charilaou, J. F. Löffler, and A. U. Gehring, Phys. Rev. B **83**, 224414 (2011).
[43]K. Binder and A. P. Young, Rev. Mod. Phys. **58**, 801 (1986).
[44]K. H. Fischer and J. A. Hertz, *Spin Glasses* (Cambridge Univ. Press, Cambridge, 1991).
[45]A. P. Ramirez, Nat. Phys. **4**, 442 (2008).
[46]L. Balents, Nature (London) **464**, 199 (2010).
[47]F. L. Pratt, P. J. Baker, S. J. Blundell, T. Lancaster, S. Ohira-Kawamura, C. Baines, Y. Shimizu, K. Kanoda, I. Watanabe, and G. Saito, Nature (London) **471**, 612 (2011).
[48]P. G. Debenedetti and F. H. Stillinger, Nature (London) **410**, 259 (2001).
[49]H. Shintani and H. Tanaka, Nat. Phys. **2**, 200 (2006).
[50]J. F. Löffler, Intermetallics **11**, 529 (2003) [reprinted from *The Encyclopedia of Materials: Science and Technology* (Pergamon/Elsevier Science, Amsterdam)].
[51]M. E. Lines, Phys. Rev. B **15**, 388 (1977).
[52]S. Ishihara, J. Phys. Soc. Jpn. **79**, 011010 (2010).
[53]N. Choudhury, L. Walizer, S. Lisenkov, and L. Bellaiche, Nature (London) **470**, 513 (2011).
[54]M. J. Harris, S. T. Bramwell, D. F. McMorrow, T. Zeiske, and K. W. Godfrey, Phys. Rev. Lett. **79**, 2554 (1997).
[55]G. Aeppli and P. Chandra, Science **275**, 177 (1997).
[56]A. P. Ramirez, in *Handbook of Magnetic Materials*, edited by K. J. H. Buschow (New Holland, New York, 2001), pp. 423–520.
[57]P. Schiffer, Nature (London) **420**, 35 (2002).
[58]A. P. Ramirez, Nature (London) **421**, 483 (2003).
[59]R. Moessner and A. P. Ramirez, Phys. Today **59**(2), 24 (2006).
[60]R. F. Wang, C. Nisoli, R. S. Freitas, J. Li, W. McConville, B. J. Cooley, M. S. Lund, N. Samarth, C. Leighton, V. H. Crespi, and P. Schiffer, Nature (London) **439**, 303 (2006).
[61]S. T. Bramwell and M. J. P. Gingras, Science **294**, 1495 (2001).
[62]P. Robinson, R. J. Harrison, S. A. McEnroe, and R. B. Hargraves, Nature (London) **418**, 517 (2002).
[63]C. Frandsen, B. P. Burton, H. K. Rasmussen, S. A. McEnroe, and S. Mørup, Phys. Rev. B **81**, 224423 (2010).
[64]R. J. Harrison, Geochem. Geophy. Geosy. **10**, Q02Z02 (2009).
[65]M. Charilaou, K. K. Sahu, S. Zhao, J. F. Löffler, and A. U. Gehring, Phys. Rev. Lett. **107**, 057202 (2011).
[66]P. Fischer, G. Frey, M. Koch, M. Könnecke, V. Pomjakushin, J. Schefer, R. Thut, N. Schlumpf, R. Bürge, U. Greuter, S. Bondt, and E. Berruyer, Physica B **276**, 146 (2000).
[67]J. Rodríguez-Carvajal, Physica B **192**, 55 (1993).
[68]A. S. Wills, Physica B **276**, 680 (2000), program available at http://www.ccp14.ac.uk.
[69]M. Rotter and A. T. Boothroyd, Phys. Rev. B **79**, 140405(R) (2009).
[70]A. T. Boothroyd, J. M. Reynolds, N. H. Andersen, E. Brecht, T. Wolf, and A. J. S. Chowdhury, Phys. Rev. B **60**, 1400 (1999).
[71]M. Rotter *et al.*, McPHASE, a software package for the calculation of phase diagrams and magnetic properties of rare-earth systems, 2002-2008, available at http://www.mcphase.de.
[72]H. Kato, Y. Yamaguchi, M. Ohashi, M. Yamada, H. Takei, and S. Funahashi, Solid State Commun. **45**, 669 (1983).
[73]Y. Yamaguchi, H. Kato, H. Takei, A. I. Goldman, and G. Shirane, Solid State Commun. **59**, 865 (1986).
[74]E. K. H. Salje, B. Wruck, and H. Thomas, Z. Phys. B: Condens. Matter **82**, 399 (1991).
[75]S. A. Hayward and E. K. H. Salje, J. Phys.: Condens. Matter **10**, 1421 (1998).
[76]S. A. Hayward, S. A. T. Redfern, and E. K. H. Salje, J. Phys.: Condens. Matter **14**, 10131 (2002).
[77]M. A. Carpenter, Am. Mineral. **91**, 229 (2006).
[78]A. V. Andreev and S. Daniš, *Proceedings of the CSMAG'07 Conference, Košice, July 9-12, 2007*, Acta Phys. Pol. A **113**, 239 (2008).
[79]A. Lindbaum and M. Rotter, in *Handbook of Magnetic Materials*, edited by K. H. J. Buschow and E. P. Wohlfarth, Vol. 14 (Elsevier Sci. Pub., Amsterdam, 2002), pp. 307–362.
[80]N. C. Wilson, J. Muscat, D. Mkhonto, P. E. Ngoepe, and N. M. Harrison, Phys. Rev. B **71**, 075202 (2005).
[81]M. Rotter, M. Loewenhaupt, M. Doerr, A. Lindbaum, H. Sassik, K. Ziebeck, and B. Beuneu, Phys. Rev. B **68**, 144418 (2003).
[82]R. J. Harrison, S. A. McEnroe, P. Robinson, B. Carter-Stiglitz, E. J. Palin, and T. Kasama, Phys. Rev. B **76**, 174436 (2007).
[83]J. R. L. de Almeida and D. J. Thouless, J. Phys. A: Math. Gen. **11**, 983 (1978).